Molecular Dynamics Simulation of MHC–Peptide Complexes as a Tool for Predicting Potential T Cell Epitopes[†,‖]

Didier Rognan,[*,‡] Leonardo Scapozza,[‡] Gerd Folkers,[‡] and Angelika Daser[§]

Department of Pharmacy, Swiss Federal Institute of Technology (ETH), CH-8057 Zürich, Switzerland, and Deutsches Rheumaforschungszentrum, D-13353 Berlin, Germany

Received January 24, 1994; Revised Manuscript Received June 13, 1994[⊛]

ABSTRACT: The class I major histocompatibility complex-encoded HLA-B*2705 protein was simulated in complex with six different peptides exhibiting unexpected structure–activity relationships. Various structural and dynamical properties of the solvated protein–peptide complexes (atomic fluctuations, solvent-accessible surface areas, hydrogen bonding pattern) were found to be in qualitative agreement with the available binding data. Peptides that have been experimentally shown to bind to the protein remained tightly anchored to the MHC molecule, whereas nonbinders were significantly more weakly complexed to the protein and progressively dissociate from it at their N- and C-terminal ends. The molecular dynamics simulations emphasize the unexpectedly important role of secondary anchors (positions 1 and 3) in influencing the MHC-bound conformation of antigenic nonapeptides. Furthermore, it confirms that dominant anchor residues cannot solely account for peptide binding to a class I MHC molecule. The molecular dynamics method could be used as a complementary tool to T cell epitope predictions from the primary sequences of proteins of immunological interest. It is better suited to MHC proteins for which a crystal structure already exists. Furthermore, it may facilitate the engineering of T cell epitopes as well as the rational design of new MHC inhibitors designed to fit optimally the peptide binding cleft.

Class I MHC[1] molecules are polymorphic glycoproteins whose function is to recognize intracellular antigenic peptides and present them at the surface of infected cells to cytotoxic T lymphocytes (Zinkernagel & Doherty, 1974; Townsend & Bodmer, 1989; Bjorkman & Parham, 1990; Madden & Wiley, 1992; Rammensee et al., 1993). As T cell receptors are normally tolerant to naturally occurring class I MHC–peptide pairs, the presentation of binary complexes with foreign peptides to T lymphocytes is a key step in the immune surveillance of intracellular pathogens. Recently, the sequences of self-peptides bound to several class I MHC proteins have been identified after HPLC elution from purified MHC molecules and Edman degradation (Falk et al., 1991; Jardetzky et al., 1991, Hill et al., 1992; Guo et al., 1992) or mass spectrometry analysis (Hunt et al., 1992; Huczko et al., 1993). Most of the class I MHC-bound self-peptides are nonamers and are anchored to the protein by conserved amino acids that are often located at positions 2 and 9 of the peptide sequence (Falk et al., 1991). Amino acids at other positions are more variable and should either contact the T cell receptor (TCR-anchor residues) or be devoid of any important binding role in the ternary class I MHC–peptide–TCR physiological complex. The location of MHC-binding residues was unambiguously determined by X-ray diffraction studies of class I MHC proteins either in complex with a mixture of bound ligands (Saper et al., 1991; Madden et al., 1992) or bound to single peptides (Silver et al., 1992; Fremont et al., 1992; Matsumura et al., 1992; Zhang et al., 1992; Madden et al., 1993; Young et al., 1994). In many class I MHC crystal structures, bound peptides present an extended conformation with charged N- and C-terminal residues tightly anchored to conserved amino acids of the MHC protein, and with the central part (from residues 4–8) protruding from the binding groove. The side chains of dominant anchor residues strongly interact with polymorphic complementary pockets and provide the molecular basis for allele-specific recognition of antigenic peptides (Guo et al., 1993; Colbert et al., 1993).

These binding rules may, however, not be obeyed for some potential T cell epitopes as recently shown for HLA-B*2705 binding peptides from the 57-kDa heat shock protein of *Chlamydia trachomatis* (Daser et al., 1994). HLA-B27 is a class I MHC molecule that is strongly associated with reactive arthritis [for a recent review, see Kingsley and Sieper (1993)], a disease which is triggered by nonspecific urethritis following bacterial infection. *C. trachomatis* has been identified as one important initiating bacteria (Kingsley & Sieper, 1993), its 57-kDa heat shock protein including six HLA-B27 binding nonapeptides (Daser et al., 1994) potentially able to elicit a CTL response.

The HLA-B*2705 peptide binding motif has been characterized by HPLC elution and microsequencing analysis of a pool of endogenous self-peptides (Jardetzky et al., 1991; Rötszchke et al., 1994). Position 2 (P2), defined as a dominant anchor residue, is always an arginine. Positions 1, 3, and 9 provide the other main anchoring positions with a significant preference for positively charged amino acids (K, R) at P1, hydrophobic amino acids (W, F, Y, I, L) at P3, and hydrophobic (L, F, Y, I, L) or positively charged residues (R, K, H) at P9. This motif is in full agreement with the high resolution crystal structure of HLA-B27 in which peptide no. 1 (RRIKAITLK, see Table 1) was modeled (Madden et al., 1992). The Arg2 and Lys9 anchor side chains make salt

[†] This work has been supported by the Schweizerischer Nationalfonds (Project No. 31-35977.92).

[‖] The six energy-minimized time-averaged structures, MD1, MD2, MD3, MD4, MD5, and MD6, have been deposited in the Brookhaven Protein Data Bank under the identification codes 1ROG, 1ROH, 1ROI, 1ROJ, 1ROK, and 1ROL, respectively.

* Author to whom correspondence should be addressed at the Department of Pharmacy, Swiss Federal Institute of Technology (ETH), Room I17M50, Winterthurerstrasse 190, CH-8057 Zürich, Switzerland (Fax: +41.1.262.15.80).

[‡] Swiss Federal Institute of Technology.

[§] Deutsches Rheumaforschungszentrum.

[⊛] Abstract published in *Advance ACS Abstracts,* September 1, 1994.

[1] Abbreviations: MHC, major histocompatibility complex; HLA, human leukocyte antigen; TCR, T cell receptor; CTL, cytotoxic T lymphocyte; Hsp, heat shock protein; MD, molecular dynamics; rms, root mean square.

0006-2960/94/0433-11476$04.50/0

Table 1: Binding of Bacterial Peptides to HLA-B*2705

no.	sequence[a]	origin	binding[b]	reference
1	RRIKAITLK	–[c]	nd[d]	Madden et al. (1992)
2	QRLKEAAEK	Hsp75 (*E. coli*)	+	Hunt and Morimoto (1985)
3	RRKAMFEDI	Hsp57 (*C. trachomatis*)	++	Daser et al. (1994)
4	ERLAKLSGG	Hsp57 (*C. trachomatis*)	–	Daser et al. (1994)
5	LRDAYTDML	Hsp57 (*C. trachomatis*)	–	Daser et al. (1994)
6	RRKAMFED	Hsp57 (*C. trachomatis*)	+	Daser et al. (1994)

[a] Strong anchor residues are underlined. [b] Binding efficiency determined by Daser et al. (1994) in an *in vitro* assembly assay and defined as the peptide concentration required for half-maximum binding (++, binding affinity lower than 1 μM; +, binding affinity between 1 and 20 μM; –, no detectable binding). [c] Peptide model fitted in the extra electron density map produced by self-nonapeptides, in the crystal structure determination of HLA-B27 (Madden et al., 1992). [d] Not determined.

bridges and hydrogen bonds to complementary negatively charged MHC pockets B and F [nomenclature from Saper et al. (1991)] whereas Ile3 is interacting with the upper part of the hydrophobic pocket D.

These experimental data do not, however, entirely account for the HLA-B27 binding properties of a set of bacterial peptides listed in Table 1. For example, peptide no. 5 (LRDAYTDML) fits the consensus sequence but is not recognized by the HLA-B27 protein. Contrarywise, octapeptide no. 6 (RRKAMFED) does not present the expected binding motif but does bind to the protein. To rationalize these structure–activity relationships, we have simulated, by molecular dynamics, the HLA-B*2705 protein in complex with six peptides presenting different MHC-binding properties. The complex with peptide no. 1, described in the crystal structure published by Madden et al. (1992), was chosen in order to derive the best MD parameters for reproducing the experimental structure and MHC–peptide interactions. Peptides no. 2 (QRLKEAAEK) and no. 3 (RRKAMFEDI) were selected as positive controls (good binders, with an Arg at P2 and expected residues at P9) while peptide no. 4 (ERLAKLSGG) was selected as a negative control (nonbinder, with incorrect residue at P9). Peptides no. 5 and no. 6 were chosen as examples where the HLA-B27 binding could not be explained by the previously described binding motifs (Jardetzky et al., 1991; Rötszchke et al., 1994). Here we document the structural and dynamic properties of each complex with respect to the MHC-binding potency of the corresponding peptide.

MATERIALS AND METHODS

Programs and Parameters. Molecular mechanics and dynamics simulations were performed using the AMBER 4.0 program (Weiner et al., 1984) and the standard parm91 parameter set (Pearlman et al., 1992). All calculations were run on a CRAY Y-MP/264. The analysis of molecular dynamics simulations were achieved using in-house routines (Krug, 1991), and animation of atomic trajectories was obtained with the MD Display program (Callahan et al., 1993).

Coordinate Setup. Starting coordinates were taken from the crystal structure of HLA-B*2705, solved at 2.1-Å resolution (Madden et al., 1992) and deposited in the Brookhaven Protein Data Bank (Bernstein et al., 1977) with the entry 1HSA. All MHC-bound nonamers were built from the peptide (ARAAAAAAA) modeled in the crystal structure, by simply substituting alanine by the corresponding residue, using the SYBYL molecular modeling package (TRIPOS Assoc., Inc., St. Louis, MO). Side chains, located according to the peptide electron density map, were centered in their respective binding pocket for MHC-binding residues or directed toward the solvent for TCR-binding amino acids. With the exception of octapeptide no. 6, the crystallographically determined peptide backbone conformation was taken as template. The C-terminal Asp residue of peptide no. 6 probably does not play the same binding role as either the P8 or P9 positions of standard nonapeptides since P8 is not a strong MHC-binding residue and the P9 side chain normally interacts with two negatively charged Asp residues in pocket F (Asp77, Asp116). Its docking in the binding cleft was based on the hypothesis that side chain oxygen atoms at the new P8 C-terminus (OD1, OD2) may replace the C-terminal carboxylate (O,OXT) of standard nonapeptides. However, none of the four polar oxygens should be in the neighborhood of Asp77 and Asp116 to avoid a strong electrostatic repulsion that may expel the P8 amino acid from the binding groove. To build peptide no. 6, the X-ray backbone conformation of nonapeptides was truncated at P9. The bulging P4–P7 part was only modeled in a more extended conformation in order to bring the P8 position to the opening of pocket F, within hydrogen-bonding distances of Tyr84(OH), Thr143(OG1), and Lys146(NZ).

In order to save computational time, only the antigen-binding α1–α2 domains were taken into account in the study. This approximation was previously shown not to alter the accuracy of the MD simulations (Rognan et al., 1992a,b; Zimmermann et al., 1992) because only limited interactions exist between the α1–α2 part and the other two domains (α3 and β_2m) that do not significantly contact peptides in the binding groove. The C-terminal residue of the α2 domain (Thr182) was protected by an N-methyl group to avoid unrealistic electrostatic interactions. Six crystal water molecules were explicitly taken into account, as they are located in the peptide binding cleft and bridge the binding of the peptide to the protein in the X-ray structure. Polar hydrogen atoms were then added, and the complexes were centered in a 7.5-Å thick shell of TIP3P water molecules (Jorgensen et al., 1983) without positional constraint on solvent atoms. Any water atom closer than 1.75 Å to any solute atom was discarded, so that approximately 1500 water molecules were added to each MHC–peptide binary complex.

Molecular Mechanics and Dynamics Protocols. Since explicit water molecules were taken into account, a dielectric constant of 1 was used. To avoid splitting dipoles, nonbonded interactions were calculated within a residue-based cutoff of 9.0 Å. The solvent atoms were first relaxed by 1000 steps of steepest descent energy minimization, the solute being held fixed. The solvated complex was then fully minimized by 1000 steps of steepest descent followed by a conjugate gradient minimization procedure until the rms gradient of the potential energy was less than 0.25 kcal/mol·Å. The minimized coordinates were thereafter used as starting point for a MD simulation at constant temperature. Initial velocities were taken from a Maxwellian distribution at 50 K, and an integration step of 2 fs was used. The system was progressively

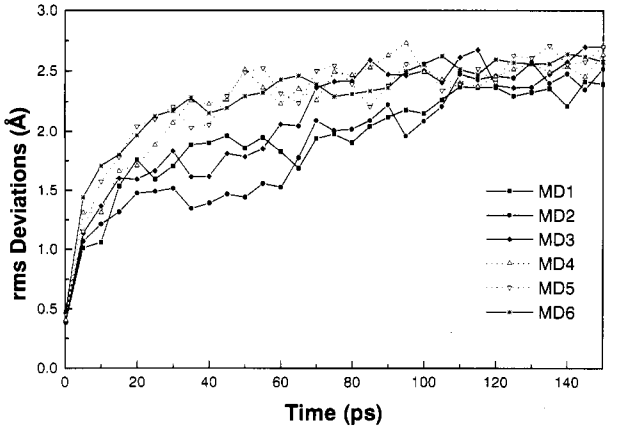

FIGURE 1: rms deviations of HLA-B27 backbone atoms from the crystal structure. MDn represents simulated HLA-B27 in complex with the bacterial nonapeptide n.

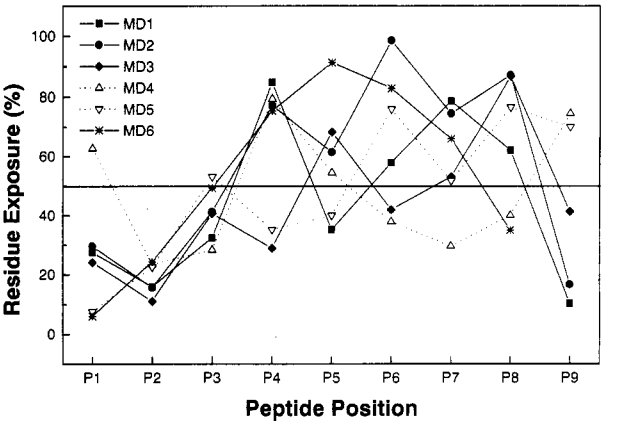

FIGURE 2: Solvent-accessible surface area of MHC-bound nonapeptides. All values were computed for relaxed MD mean structures, time-averaged over 500 conformations during the last 50 ps of the simulations.

heated from 50 to 297 K during the first picosecond, the temperature being held at 297 K for the rest of the simulation by coupling the system to a heat bath (Ryckaert et al., 1977) using a temperature coupling constant of 0.05 ps. All bond lengths were constrained to their equilibrium values using the SHAKE algorithm (Berendsen et al., 1984) with a bond length tolerance of 2.5×10^{-4}. Coordinates, energies, and velocities were collected and saved every 50 steps (0.1 ps) for 150 ps. Each 150-ps MD simulation required 22 CPU hours on a CRAY Y-MP/264.

Solvent-Accessible Surface Areas. Accessible and buried surface areas were computed on energy-minimized mean structures, by using the MS program (Connolly, 1983) with a 1.4-Å radius probe. For expressing results in percentage of residue exposure, similar computations were done on free Gly-Xaa-Gly tripeptides built in a fully extended conformation. For peptide N- and C-termini, charged Xaa-Gly-Gly and Gly-Gly-Xaa tripeptides were used as templates, respectively. The solvent accessibility of residue Xaa was determined as the ratio of the accessible surface area of the residue in the MHC-bound nonapeptide to that in the free tripeptide.

RESULTS

Throughout the study, active peptides will refer to sequences that experimentally bind to the HLA-B*2705 protein whereas inactive peptides do not present any detectable binding to the MHC protein in an *in vitro* assembly assay (Daser et al., 1994).

RMS Deviations. A standard way to appreciate the quality of a MD simulation is to monitor the instantaneous deviation of simulated structures from the experimental starting conformation throughout the computation. Figure 1 shows the rms positional deviations of HLA-B27 backbone atoms from the crystal structure, when simulated in complex with six peptides, four binding (nos. 1, 2, 3, and 6) and two nonbinding (nos. 4 and 5) sequences. All deviations reach a plateau at 2.5 ± 0.2 Å but are still drifting slightly. Longer simulations (200 ps) for peptides 1 and 2 did not affect the averaged rms deviation value (data not shown). Similar values were found when time-averaged MHC conformations are compared. Deviations of the peptide backbone from its experimental structure are relatively low for active peptides (0.7 Å for peptide no. 1, 0.90 Å for peptide no. 2, 1.2 Å for peptide no. 3; no comparison can be made for octapeptide no. 6) but significantly higher (1.5–2.0 Å) for inactive peptides 4 and 5.

MD simulations using different force fields, atomic models (united or all atom), solvation types (water shell of different sizes, water box with periodic boundary conditions), and nonbonded cutoff values (9–12 Å) produced MHC–peptide structures that were not significantly closer to the crystallographically determined structure (unpublished results).

Solvent-Accessible Surface Areas. The calculations were performed using a probe radius of 1.4 Å for simulating water molecules. The results have been expressed in fragmental solvent-accessible surface areas (see Materials and Methods) for a direct quantitation of MHC-bound peptide residue exposure. MHC-binding positions could be very well identified using this method. They are reported in Figure 2 for all HLA-B27-bound peptides in their time-averaged conformations between 100 and 150 ps. The four binding peptides (nos. 1, 2, 3, and 6) have their first three amino acids and the C-terminal residue buried (less than 50% of residue exposure) upon HLA-B27 binding. This confirms the anchoring role of these positions especially at P2 and at the C-terminus (P8 or P9), the two main anchor residues that are extensively buried. A C-terminal isoleucine (peptide no. 3) is, however, more accessible to water than a lysine (compare peptides 1 and 2). The middle part (P4–P8 for nonamers, P4–P7 for the octamer) bulges from the binding groove and does not strongly interact with the protein. As a consequence it is much more accessible to solvent.

Inactive peptides 4 and 5 present a highly exposed C-terminal amino acid (residue exposure about 70%). A similar effect is found at the N-terminus but only for peptide no. 4 (P1 = Glu), the nonamer no. 5 exhibiting an opposite profile (P1 = Leu, residue exposure of 8%). As previously described for binding peptides, the solvent accessibility of the middle section (P4–P8) is much higher but difficult to correlate with the sequence of the corresponding peptides. The solvent accessibility pattern of the P6–P8 part of peptide no. 4 (Leu-Ser-Gly) is, however, reversed with respect to that of all other sequences.

RMS Atomic Fluctuations. The atomic fluctuations of the six HLA-B27 pockets were computed and compared to the fluctuations calculated from the crystallographically determined temperature factors, in order to illustrate the flexibility of the antigen binding subsites and identify those which are the more strongly bound to peptide side chains (Figure 3). In the crystal structure described by Madden et al. (1992), the two strongest anchor residues (P2, P9) specifically interact with the polymorphic pockets B and F.

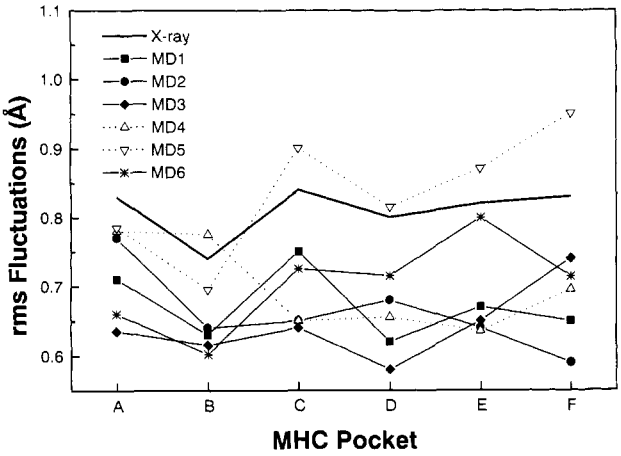

FIGURE 3: rms atomic fluctuations of the six HLA-B27 specificity pockets (side chain atoms only) for HLA-B27 in complex with bacterial peptides 1–6. The values for the X-ray structure (bold line) were obtained from the crystallographic temperature factors and converted to Å units. Fluctuations were calculated from time-averaged conformations over the last 500 conformations. The pockets definition was done according to Saper et al. (1991) as follows: pocket A (Met5, Tyr7, Tyr59, Glu63, Tyr159, Glu163, Trp167, Tyr171), pocket B (His9, Thr24, Glu45, Leu66, Cys67, Tyr99), pocket C (His9, Lys70, Thr73, Asp74, Arg97), pocket D (Tyr99, His114, Leu156, Tyr159, Leu160), pocket E (His114, Trp133, Trp147, Val152, Leu156), pocket F (Asp77, Thr80, Leu81, Tyr84, Asp116, Tyr123, Thr143, Lys146, Trp147).

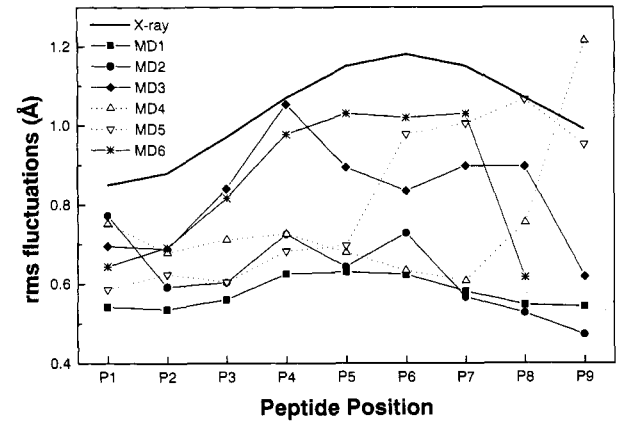

FIGURE 4: rms atomic fluctuations of HLA-B27-bound peptides (backbone atoms) for the crystal structure and six MD conformations. Fluctuations were calculated as indicated in Figure 3 and averaged per residue.

Secondary anchor residues (P1, P3) are directed toward pockets A and D, respectively. A very similar binding mode is observed when HLA-B27 is bound to active peptides (nos. 1, 2, 3, and 6), the pockets B, D, and F presenting the lowest atomic fluctuations. The calculated atomic motions fluctuate in a similar manner to those derived from the *B* factors, but the magnitude differs. When bound to the inactive peptide no. 4, the rms positional fluctuations of the six pockets are very similar to those observed for antigenic complexes, with the exception of pocket B (interacting with arginine at P2) that shows an enhanced mobility. In complex with peptide no. 5, this situation is even more strengthened since all specificity subsites present dramatically increased atomic fluctuations, especially pocket F that normally interacts with the anchor P9 position. In most of the cases, the atomic motions of the specificity pockets are highly related to that of their complementary peptide side chains (compare Figures 3 and 4) especially for the P9 position of inactive peptides 4 and 5 which seems to be only weakly anchored to pocket F. It can be noticed that the highest rms atomic fluctuation values observed for pocket B are found when the HLA-B27 molecule is complexed with inactive peptides.

A complementary picture of the atomic motions of MHC-bound peptides is displayed by Figure 4. Active peptides 1 and 2 present uniformly low fluctuations all along their sequence especially for the two anchor amino acids P2 and P9. After a peak at P4 whose side chain is directed toward solvent in both X-ray and MD structures, the atomic fluctuations progressively decrease until the C-terminal amino acid is reached. Here again, the calculated fluctuations are in rather good agreement with the experimental values, unless they are 0.3–0.5 Å lower. The peptide no. 3 shows a similar pattern except at P4 and importantly at P9 that is much more flexible than expected. This observation is compatible with the previously calculated solvent-accessible surface areas of the C-terminus of all active peptides (recall Figure 2) that indicate different binding capacities of isoleucine (peptide no. 3) and lysine (peptides 1 and 2) to the MHC pocket F. Both termini of peptide no. 4 are highly flexible, the rest of the sequence exhibiting a mobility similar to that of active peptides. Peptide no. 5 presents significantly enhanced atomic fluctuations for the whole C-terminal half of the sequence. Interestingly, octapeptide no. 6 when bound to the HLA-B27 protein shows low atomic fluctuations only at P1 and P2 and at the C-terminal P8 amino acid, confirming the binding role of these three positions for the octamer.

MHC–Peptide Interactions. Two criteria have been selected for describing a hydrogen bond: a donor (D) to acceptor (A) distance lower than 3.2 Å and a D–H···A angle value in a 140–180° range. Fifteen hydrogen bonds have been identified in the HLA-B27-peptide crystal structure. They involve mainly the two main anchor residues (P2, P9) and their complementary polymorphic pockets (B and F). Arg2 is strongly bound to four polar MHC residues (His9, Thr24, Glu45, and Tyr99), two interactions being bridged by a water molecule. Lys9 is interacting with two negatively charged HLA-B27 residues (Asp77 and Asp116) of pocket F. Both charged termini are hydrogen-bonded to highly conserved MHC amino acids at the two ends of the peptide binding groove (Tyr7, Tyr59, Tyr171 for the N-terminus; Tyr84, Thr143, Lys146 for the C-terminus).

The time-averaged MD structure of peptide no. 1 was bound to the protein as in the starting crystal structure. A total of 18 hydrogen bonds were identified (Table 2). Only four original interactions have been lost, but they were replaced by new bonds involving either neighboring atoms of the former MHC residue partner or new HLA amino acids in the close vicinity of the previous ones. For example, the N-terminus is differently bound in the MD structure of peptide no. 1, one starting partner (Tyr171) being replaced by a new one (Tyr59). Furthermore, the N-terminus develops a water-bridged hydrogen bond with Glu63 that was absent in the crystal structure (Figure 5A). The solvent molecule (Wat461) engaged in this interaction is one of the six water molecules that were explicitly described in the crystal structure. This water intercalation effect around the peptide N-terminus was already found when HLA-A2 was simulated in complex with viral nonapeptides (Rognan et al., 1992b; Rognan & Folkers, 1993) and may reflect differences between MHC–peptide structures in the crystal state and in solution. All other interactions involving the two main anchor residues were reproduced by the simulation or even strengthened as for the P9 lysine interacting with pocket F.

The active peptide 2 is similarly bound to the protein. Sixteen MHC–peptide hydrogen bonds were found in the MD

Table 2: MHC–Peptide Hydrogen Bonds[a]

peptide	HLA*B2705	X-ray	MD1	MD2	MD3	MD4	MD5	MD6
P1(N)	Tyr7(OH)	■	■	□	■	□	□	■
	Tyr59(OH)	□	■	■	■	□	□	□
	Glu63(OE1)	□	□	■	■	□	□	■
	Glu63(OE2)	□	□	□	□	□	■	□
	Tyr171(OH)	■	□	□	□	□	□	□
P1(NE)	Glu163(OE2)	■	□	x	□	x	x	□
P1(NH1)	Glu63(OE2)	□	■	x	■	x	x	□
P1(NH2)	Glu58(OE2)	□	■	x	□	x	x	□
	Glu166(OE2)	□	□	x	□	x	x	■
P1(O)	Tyr99(OH)	□	□	□	■	□	□	■
	Tyr159(OH)	■	■	■	□	□	■	□
P2(N)	Glu63(OE1)	■	■	□	□	□	□	□
P2(NE)	Glu45(OE1)	■	■	□	■	□	□	■
	Glu45(OE2)	□	□	■	□	□	□	□
	Glu63(OE2)	□	□	□	□	■	□	□
P2(NH1)	His9(NE2)	□	■	□	■	□	□	■
	Thr24(OG1)	■	■	■	□	□	■	□
	Glu45(OE1)	□	□	■	□	□	□	□
P2(NH2)	His9(NE2)	□	□	□	□	□	□	■
	Glu45(OE1)	■	■	■	■	□	□	□
	Glu45(OE2)	□	□	■	■	■	■	■
P2(O)	Arg62(NH1)	■	□	□	□	□	□	□
P3(N)	Tyr99(OH)	■	■	□	■	□	■	■
P3(OD2)	Gln155(NE2)	x	x	x	x	x	■	x
P3(NZ)	Asp77(OD1)	x	x	x	x	x	x	■
P8(O)	Lys146(NZ)	□	□	□	□	□	□	■
	Trp147(NE1)	■	■	■	□	□	□	□
P8(OXT))	Thr143(OG1)	x	x	x	x	x	x	■
P8(OD2)	Tyr84(OH)	x	x	x	x	x	x	■
P9(N)	Asp77(OD1)	■	■	■	□	□	■	x
P9(NZ)	Asp77(OD2)	□	■	■	x	x	x	x
	Asp116(OD2)	■	■	■	x	x	x	x
P9(O)	Tyr84(OH)	□	□	□	■	□	□	x
	Thr143(OG1)	■	□	□	□	□	□	x
	Lys146(NZ)	□	■	■	□	□	□	x
P9(OXT)	Tyr84(OH)	■	■	■	■	□	□	x
	Thr143(OG1)	□	■	■	□	□	□	x
	Lys146(NZ)	□	□	■	■	□	□	x
total		15	18	16	13	2	7	13
backbone		10	9	9	8	1	4	6
sidechains		5	9	7	5	1	3	7

[a] Peptide positions (Pn) are labeled from 1 (N-terminus) to 9 (C-terminus). Closed and open boxes indicate the presence or absence of a peptide–MHC hydrogen bond, respectively (time-averaged distance between donor D and acceptor A less than 3.2 Å, D–H···A angle between 140° and 180°). Crosses indicate the absence of specific side chains for some peptides. Hydrogen bonds have been analyzed for the crystal structure (X-ray) and during the last 50 ps of the simulation over 500 HLA–peptide conformations for each complex with peptides 1–6 (MD1–MD6).

mean structure (Table 2). Here again, the peptide N-terminus was differently hydrogen-bonded to HLA-B27 with respect to the crystal situation. One starting hydrogen bond (to Tyr7) was rapidly replaced by an interaction with Glu63, at the upper part of pocket A so that the N-terminal end of the bound peptide was slightly shifted upward in the direction of the α-helix of the α1 domain (Figure 5B). The Arg2 side chain has retained its usual binding partners even if some interacting atoms have been exchanged (OE1 for OE2 at Glu45, for example). The charged C-terminus remains anchored to the conserved Tyr84, Thr143, and Lys146, located at the rim of pocket F.

For peptide 3, fewer hydrogen bonds to the protein were found mostly by the absence of hydrogen-bond donating properties for the side chain at P9 (lysine is replaced by isoleucine; see Table 1). As a consequence, the C-terminal end has a reduced number of interactions with respect to peptides 1 and 2. The neighboring P8 position that contributes to lock the C-terminus to its binding pocket F through one usual hydrogen bond with Trp147 does not interact with the protein. To compensate this weaker hydrogen-bonding capacity, stronger van der Waals interactions are developed between the Ile9 side chain and hydrophobic amino acids of the pocket F (Leu81, Tyr123, Trp147; see Figure 5C). The first three amino acids (P1–P3) remain strongly bound to the MHC molecule with conservation of most of the hydrogen bonds found in the crystal structure. Only the P1 backbone oxygen atom has changed binding partners (Tyr99 for Tyr159).

When the MHC–peptide interactions are observed for nonbinding peptides 4 and 5, much fewer intermolecular hydrogen bonds are found (2 and 7, respectively). In both cases, the C-terminal oxygen atoms (O,OXT) have lost all of the original hydrogen bonds to the three conserved polar residues of pocket F (Figure 5D,E). The interaction provided by the N-terminal part has also been modified. The N-terminus is not bound at all for peptide no. 4, and only one hydrogen bond to Glu63 remains stable for peptide no. 5. The binding profile of Arg2 is less affected. However, its side chain is shifted toward the rim of pocket B (Glu63) for peptide no. 4. Interestingly, new hydrogen bonds to the Gln155 side chain (at the protein surface) are observed for the P3 amino acid (Asp) of peptide no. 5. The presence of a negatively charged side chain at P3 forces the peptide to adopt an intramolecular hydrogen bond to the P4 nitrogen amide that remains stable throughout the 150 ps of the MD simulation.

Thirteen MHC–peptide hydrogen bonds are observed for the octapeptide no. 6 in complex with HLA-B27 (Figure 5F). The peptide N-terminus, as previously shown for peptides 2 and 3, has been displaced in the direction of the Glu63 side chain in order to develop a salt bridge with its negatively charged oxygen atoms. The dominant anchor residue Arg2 is directly bound to two polar MHC side chains (Glu45, His9) of pocket B. An additional hydrogen bond between the NE atom of Arg2 and Glu63 side chain was found in the mean MD structure. The P3 amide nitrogen atom is hydrogen-bonded to Tyr99 as often observed for active nonapeptides. Remarkably, the side chain of Lys3 is expelled from pocket D (Tyr99, His114, Tyr159) where it was expected to be located, to point in the direction of Asp77 and to make a salt bridge with the OD1 atom of this MHC residue. The P4–P7 middle part of the octapeptide does not interact with the HLA-B27 protein, with the exception of a weak hydrophobic interaction between P5 (Met) and the MHC pocket E (His114, Val152, Leu156). The MHC-bound conformation of the C-terminus is different from that of standard MHC-bound nonapeptides. The two side chain oxygen atoms at P8 (OD1, OD2) are replacing the C-terminal carboxylate of nonapeptides. The first one is bound to Tyr84 and the second to a crystal water molecule (Wat451) bridging the binding to Tyr84 and Arg83. The C-terminal carboxylate of the octapeptide has been shifted toward the α-helix of the α2-domain and is hydrogen-bonded to Thr143.

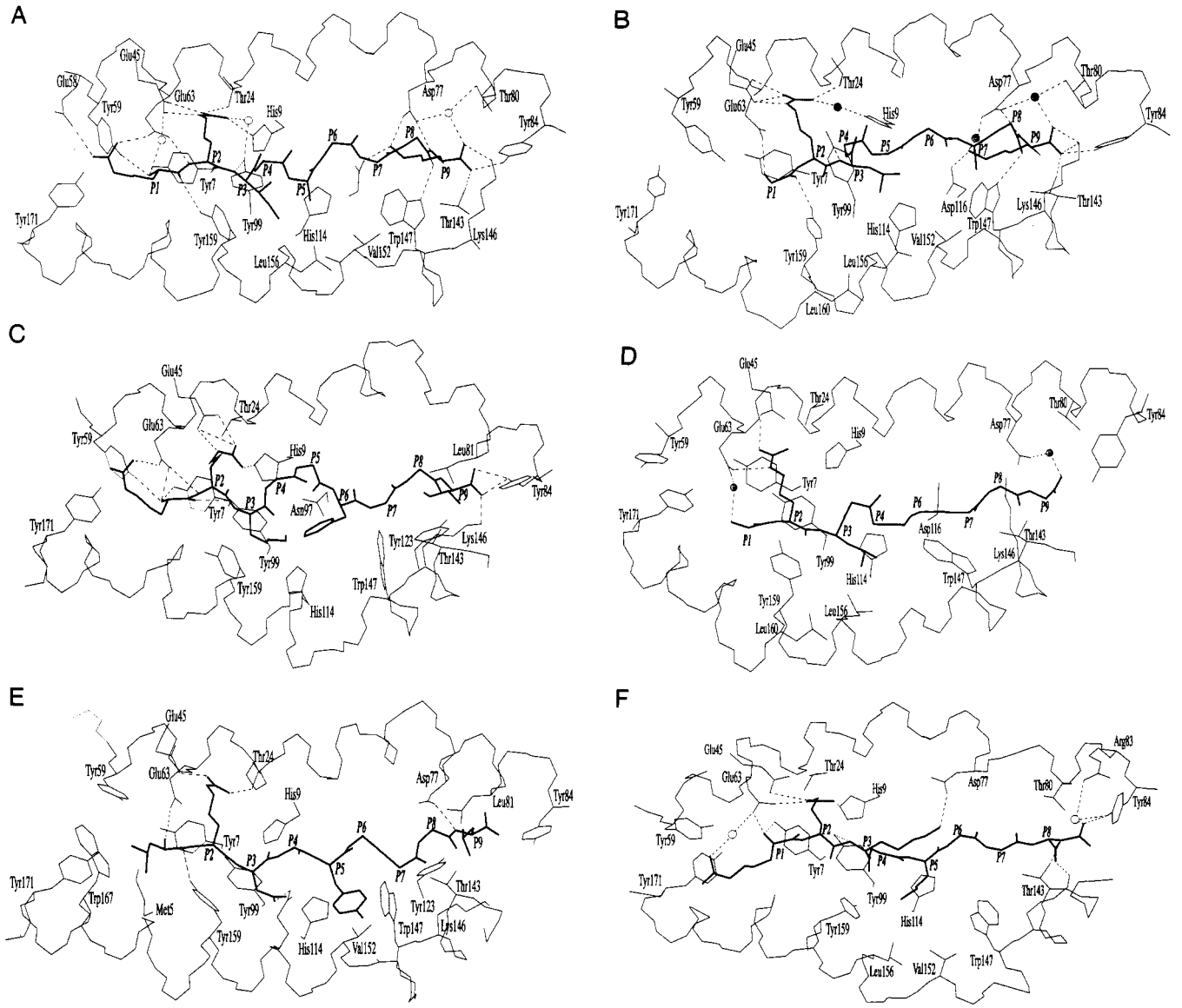

FIGURE 5: Time-averaged conformation of HLA-B27 in complex with six peptides (A, peptide 1; B, peptide 2; C, peptide 3; D, peptide 4; E, peptide 5, F, peptide 6). The backbone atoms of the two α-helices delimiting the peptide binding groove are displayed here with the side chains of peptide-binding residues. The Cα positions of bound peptides (in bold lines) are labeled from P1 (N-terminus) to P9 (C-terminus). Only the peptide anchor side chains are shown. MHC–peptide hydrogen bonds are represented by broken lines and water molecules by balls.

DISCUSSION

In this study, we were primarily interested in finding atomic properties able to distinguish binding from nonbinding nonapeptides. The MD simulations of class I MHC–peptide complexes in fact proved able to account for anomalous binding of the chosen bacterial peptides to the HLA-B27 protein. Alteration of the protein conformation upon peptide binding cannot be invoked since higher rms deviations from the crystal structure are not observed when inactive peptides are docked in the binding groove (Figure 1). The deviations that are here reported after 150 ps are consistent with previously calculated rms deviations of the simulated HLA-A*0201 protein from its crystal structure (Rognan et al., 1992b) but higher than those recently described for proteins of similar size (van Gunsteren & Mark, 1992; Kitson et al., 1993). The dimensions of the binding cleft (about 25 Å long and 10 Å wide) might explain in part the observed deviations from the crystal structure. However, by excluding solvent-exposed loops (residues 15–17, 38–45, 85–93, 104–108, 127–132) from the calculation, smaller deviations (1.7 Å) were observed.

A clearer view is obtained when the solvent-accessible surface areas of bound peptides are computed. The total peptide surface that is accessible upon HLA binding is slightly lower for HLA-B27-binding peptides (about 400 Å^2) than for inactive peptides (averaged value of 450 Å^2). The difference is more significant when only the MHC-anchoring positions (P1, P2, P3, and P8 or P9) are considered (mean value of 102 Å^2 for peptides 1, 2, 3, and 6 against 170 Å^2 for peptides 4 and 5). This observation is in agreement with the correlation reported by Saito et al. (1993) between the buried surface areas of H-2K^b-binding octapeptides and their dissociation constants. The inactive peptide no. 4, initially chosen as a negative test (wrong residue at P9), could be detected as an outlier with respect to three binding nonapeptides. Both terminal ends of this peptide are clearly dissociating from their MHC subsites (pocket A and F) as shown by their unusually high accessible surface areas. This observation is explained by the sequence of this peculiar peptide (ER-LAKLSGG), specifically the combination of a glutamic acid at P1 and a glycine at P9. As P9 is a strong anchor position, the absence of either a positively charged (Lys, Arg) or

hydrophobic side chain (L,Y), which are predominantly found in the sequence of self-peptides (Jardetzky et al., 1991; Rötzschke et al., 1994), induces a dissociation of the C-terminal end from its binding subsite. The other inactive peptide no. 5 (LRDAYTDML), in spite of expected amino acids at P2 and P9, also presents a highly exposed C-terminus. Remarkably, secondary anchors P1 (Leu) and P3 (Asp) have an unusual exposure to solvent. The leucine is much more buried than expected whereas Asp is the only P3 amino acid that is rather accessible to the solvent. It can be noticed that both Leu1 and Asp3 have not been detected in the sequence of self-peptides eluted form purified HLA-B*2705 (Jardezky et al., 1991; Rötzschke et al., 1994).

Atomic fluctuations of either MHC binding subsites or bound peptide amino acids have been considered in Figures 3 and 4. In both cases, rms fluctuations derived from the experimental *B* factors are 0.3–0.5 Å higher than those computed from MD trajectories. These discrepancies have been reported in many MD simulations and are probably due to the equation that converts thermal factors into rms fluctuations (Karplus & Petsko, 1990). Since anharmonic and anisotropic motions have been neglected here, experimentally derived fluctuations are overestimated by at least 0.3–0.4 Å (Karplus & McCammon, 1983). The atomic fluctuations of peptide amino acids vary in parallel with that of their complementary pocket. For active peptides 1 and 2, P2 and P9 anchor residues as expected fluctuate less than the noninteracting part of the sequence. A complementary observation was made for the specific MHC pockets, where the antigen-binding pockets (B and F) exhibit lower fluctuations than the remaining four that do not interact as strongly with the nonapeptides. It clearly shows that both anchor positions are tightly bound to their respective subsites. A noticeable difference is, however, found for peptide no. 3, which has an isoleucine at P9. An hydrophobic amino acid seems to develop a weaker interaction than a positively charged lysine, as demonstrated by higher values obtained for both the accessibility to water and the atomic fluctuations of the P9–pocket F pair. This makes sense in terms of the free enthalpy of binding that is certainly favored for a lysine that can make buried salt bridges to its complementary pocket F (with two aspartic acid at positions 77 and 116). However, the fact that peptide no. 3 is a good binder (Daser et al., 1994) is somewhat in contradiction with our observed atomic properties at P9. To reconcile both results, it may be hypothesized that some unfavorable contributions (free energy of desolvation, entropic component ΔS) balance the better free enthalpy of binding (ΔH) provided by a lysine amino acid at P9. Thus, the resulting free energy of binding (ΔG) may be quite similar for lysine and isoleucine residues. Such a bivalent preference for either positively charged or hydrophobic amino acids is unusual in peptide selection by class I MHC proteins (Falk et al., 1991) and is difficult to rationalize by simple force field calculations. Free energy perturbation methods may solve this problem by computing the free energy change $\Delta\Delta G$ associated to a single point mutation (Lys → Ile) at the P9 position of a HLA-B27-binding nonamer.

As demonstrated by peptide no. 5 whose sequence perfectly fits the HLA-B27 binding motif, the presence of the two main anchor residues (P2, P9) is necessary but not sufficient for binding to the protein. The rms atomic fluctuations of the solvated complex no. 5 provides a molecular explanation for this unexpected observation. The C-terminal half of this peptide (P6–P9) as well as its corresponding binding pockets (C, E, and notably F) have unusually high atomic motions when compared to active MHC–peptide pairs. One cause may be the presence of an aspartic acid at P3. A side chain at this secondary anchor position is normally directed toward the upper aromatic part of pocket D (Tyr99, Tyr159). P3 is located after the first dominant anchor position (P2) and just before the kink in the backbone conformation that allows the P4–P8 section to bulge from the binding groove and probably interacts with a T cell receptor (Madden & Wiley, 1992). It is likely that hydrophobic amino acids (F, I, L, V, A, W, Y) that are preferentially found at this position in self-peptides (Jardetzky et al., 1991; Rötzschke et al., 1994) contribute to the stabilization of the peptide in the binding groove by direct van der Waals contacts with the upper part of pocket D and by stabilizing the interaction of Arg2 with its binding pocket B. Since pocket D is rather deep, it cannot be fully occupied by natural amino acids at P3, assuming that all nonapeptides bind in very similar conformations to class I MHC proteins, at least for the P1–P3 part. This observation may explain why no absolute preference is found at the P3 position of self-peptides eluted from HLA-B27. When a negatively charged amino acid (Asp, Glu) is located at this position, whether or not the binding motif has been fulfilled, repulsion with the upper part of pocket D causes the rest of the sequence (P4–P9) to be expelled from the binding site, especially the C-terminal residue that cannot strongly interact with its complementary subsite (pocket F). This effect can be easily seen when atomic fluctuations of the pockets D and F are observed (Figure 3). Furthermore, all chlamydial peptides with a Asp or Glu at P3 did not to bind to the HLA-B27 molecule in our *in vitro* assembly assay (Daser et al., 1994). Similar observations have been made for peptide selection by the HLA-A*0201 allele (Ruppert et al., 1993). Another effect of the loss of hydrophobic interactions between P3 and pocket D is the weakening of the interaction of the neighboring Arg2 with pocket B as suggested by the higher exposure to solvent of P2, the elevated rms atomic fluctuations of this pocket for peptide no. 5, and the analysis of the MHC–peptide hydrogen bonding pattern (Table 2). In order to study the binding role of this auxiliary anchor, we designed a series of peptides in which nonnatural side chains were incorporated at position 3, in order to optimize their interactions with pocket D. All of them were indeed found to bind with higher affinities to the HLA-B27 molecule than parent peptides bearing standard residues at P3 (manuscript in preparation). Replacing Asp by Leu and Leu by Asp at the third position of peptide no. 5 and no. 2, respectively, and testing their binding affinity to HLA-B27 is in progress to assess the binding role of a negatively charged side chain at P3.

The total number of MHC–peptide hydrogen bonds for time-averaged conformations, is directly correlated to the binding properties of the corresponding peptide (Table 2). Whereas the hydrogen-bonding pattern found in the crystal structure is quite well reproduced for all active nonapeptides, a significant loss of important hydrogen bonds is observed for inactive analogues, at both termini and to a lesser extent at the P2 position. It also illustrates the potential role of the auxiliary anchor position at P1. Positively charged amino acids (lysine, arginine) are often found at the P1 position of self-peptides eluted from HLA-B27 (Jardetzky et al., 1991; Rötzschke et al., 1994). They may provide additional hydrogen bonds or salt bridges to negatively charged residues present at the rim of pocket A (Glu58, Glu63, Glu163) so that the peptide N-terminus could be better locked to its binding pocket A. The rms atomic fluctuations of this pocket are indeed lowered when bound to a peptide bearing an arginine

Table 3: MHC–Peptide Hydrophobic Contacts

no.	sequence	side chain	buried area (Å²)[a]	HLA pocket	contact residues
1	RRIKAITLK	Ile3	82	D	Y99, L156, Y159
		Ala5	38	E	H114, V152, L156
2	QRLKEAAEK	Leu3	77	D	Y99, H114, L156
		Ala7	40	E	W147, V152
3	RRKAMFEDI	Lys3	73	D	Y99, Y159
		Phe6	88	C	N97, Y99, H114
		Ile9	110	F	L81, Y123, T123
4	ERLAKLSGG	Leu3	81	D	Y99, H114, L156
5	LRDAYTDML	Leu1	124	A	M5, Y7, W167
		Tyr5	89	E	H114, V152, W147
		Leu9	75	F	L81, Y123, T143
6	RRKAMFED	Met5	44	E	H114, V152, L156

[a] Buried surface areas were calculated on relaxed time-averaged structures using the MS program (Connolly, 1983) with a 1.4-Å probe radius.

at P1 (peptides 1, 3, and 6, Figure 3). Here again, binding studies with peptides modified only at P1 should test this hypothesis.

From this study, it is very difficult to assess the contribution to binding of the bulging part (P4–P8) of these peptides. Although the starting conformation was identical for all peptides, the orientation of the corresponding side chains (toward the binding groove or the solvent) is not absolutely conserved, except for the interaction of P3 with the upper part of pocket D (Table 3). Other side chains (P5, P6, P7) are involved in weak van der Waals contacts with central pockets (C and E) of the MHC binding cleft. Interestingly, it seems that one side chain can influence the orientation of another in the binding groove. For example, a long side chain at P3 (as lysine for peptide no. 3) reverses the direction of the P5–P6 side chains (P5 toward water, P6 toward the binding groove) with respect to the effect of a short hydrophobic amino acid (Ile, Leu) at P3. This reorganization is achieved in order to avoid steric repulsion between P3 and P5 side chains. As a consequence of the twist at P5, it is the next side chain (P6) that contacts the binding groove (Table 3). These binding rules are not fulfilled for the octapeptide no. 6 that presents a different MHC-bound conformation at the C-terminal part and a salt bridge between P3 and Asp77. The combination of different side chains at P3, P5, and P6 may then be beneficial or detrimental to the binding affinity of the peptide. Similar observations have been made from the crystal structures of single complexes between HLA-A2 and viral peptides (Madden et al., 1993).

The MD simulation not only reproduces MHC–peptide interactions occurring in the crystal state for active nonapeptides but also shows different locations of P2 and P9 anchor residues and the progressive expulsion of nonactive peptides from the binding cleft as illustrated by the solvent-accessible surface areas of active and inactive peptides. Taken together, these results corroborate the experimental data published by Burshtyn and Barber (1993) on the dynamics of peptide binding to purified H-2D^b indicating that the stability of the class I trimolecular complex (heavy chain–peptide–β_2m) is directly dependent on the peptide sequence and its binding affinity for the MHC protein. Parker et al. (1992b) also reported that the dissociation rate of the β_2 microglobulin from the trimeric complex is related to the binding affinity of the peptide to the MHC molecule.

An almost complete dissociation of inactive peptides from HLA-B27 would perhaps occur if much longer simulations had been performed. We decided to stop the MD simulation after 150 ps because this time scale was already sufficient for describing a striking difference between binding and nonbinding peptides. Complete release of the inactive peptides from the binding groove would require much longer simulations and thus limit the predictive power of the methodology since extra computational expense would be required.

In addition to the simulation of nonameric peptides, we propose a model that account for the unexpected binding potency of octapeptide no. 6. The binding role of the usual C-terminal carboxylate (for nonapeptides) is here played by a negatively charged side chain (Asp or Glu) at P8, the C-terminus being shifted to the rim of pocket F. Exactly the same MHC residues were involved in peptide binding with the exception of the positively charged Arg83 that allows the fixation of a water molecule for bridging the interaction with the peptide (Figure 5F). Other MHC–peptide interactions were highly conserved, especially the hydrogen bonding network between P2 and the pocket B of the protein. The proposed model is an alternative binding mode for octapeptides with negatively charged amino acids at P8 and a correct binding motif at other positions. It is different from the conformation of murine H-2K^b binding octapeptides, for which the bulging part is only one amino acid shorter (Fremont et al., 1992).

This study, in agreement with recent data on the binding of peptides to class I HLA-A2 and H-2k^b (Ruppert et al., 1993; Saito et al., 1993) and class II EαEβ molecules (Boehncke et al., 1993), suggests that the presence or absence of dominant anchor residues is not sufficient for explaining MHC-binding properties. Although natural T cell epitopes have already been predicted by fitting primary sequences to allele-specific binding motifs (Rötzschke et al., 1991; Pamer et al., 1991), such a method would have failed for example to predict the binding properties of peptides 5 and 6, by neglecting the influence of secondary anchor positions (P1, P3) or the possibility of a conformational rearrangement at the peptide C-terminus. Furthermore, three-dimensional informations missing in classical predictions are crucial for determining which peptide residues are involved in MHC binding and T cell recognition.

The utility of theoretical simulations as a complementary tool for interpreting biological data is well established [for recent reviews, see van Gunsteren and Berendsen (1990) and van Gunsteren and Mark (1992)]. In the field of MHC–peptide interactions, it has been possible to propose a HLA-A2-bound conformation for a viral nonapeptide and the relevant MHC–peptide interactions (Rognan et al., 1992b) fully validated by subsequent X-ray diffraction data (Madden et al., 1993). The rms deviation of the simulated MHC-bound peptide from the experimental structure was only 1.2 Å, and six out of nine MHC–peptide hydrogen bonds found in the crystal structure were predicted. In the present study, all MHC–peptide complexes were solvated in a water shell. Simulating class I MHC–peptide complexes in vacuo never led to MHC conformations and MHC–peptide interactions, similar to those found by X-ray diffraction. The explicit inclusion of six water molecules from the crystal structure is not an absolute prerequisite. Their time-averaged coordinates and the binding role of the three most important could be reproduced by solvent molecules of the AMBER water shell when they were not taken into account (unpublished results). More important is the initial conformation of MHC-binding side chains. With the exception of Arg2, all side chains have been added by substituting alanine amino acids (present in the PDB entry) by the residues corresponding to the sequence of the six peptides studied here. In all cases, the χ_1 and when possible the χ_2 dihedral angles were kept constant, so that

each MHC-binding side chain was centered in its binding pocket. When steric or electrostatic repulsion with the protein were absent, small differences in the starting coordinates of the MHC-bound peptide side chains did not significantly modified the results presented in this report. The only arbitrary choice in the peptide conformation concerns the TCR-binding side chains (P4 and P8), which were always oriented toward the solvent, with no interactions with the HLA-B27 protein. Even if a complete MHC-bound peptide structure has been available, fitting all peptide side chains to an experimentally determined structure would no doubt also have generated partially incorrect structures, since each P4–P8 peptide sequence probably has a different conformation, as demonstrated by the crystal structures of four viral nonapeptides bound to HLA-A2.1 (Madden et al., 1993). Of course, MD conformations cannot replace structures that have been experimentally determined. They do, however, provide simple models for explaining binding properties and structure–activity relationships and may be used for drug design purposes.

We propose that molecular dynamics simulations of MHC–peptide pairs may be an alternative and complementary tool for clarifying MHC-binding properties, extending the existing MHC-binding motifs and predicting potential T cell epitopes. The method can be applied rapidly provided that some initial conditions (ideally X-ray coordinates of a MHC–peptide pair and water solvation) are fulfilled. Simulation and analysis of one binary complex requires no more than one week on a CRAY supercomputer. It has already facilitated the rational discovery of nonnatural peptides, designed to fit optimally the peptide-binding groove (manuscript in preparation). Such molecules should be useful tools for the individual treatment of autoimmune diseases to which some class I MHC alleles are associated.

ACKNOWLEDGMENT

We thank Dr. Avrion Mitchison for critical reading of the manuscript and the Computational Center of the ETH Zürich for generous allocation of computer time. Atomic coordinates of all time-averaged structures are available upon request. D.R. may be contacted at the following e-mail address: didier@pharma.ethz.ch.

REFERENCES

Berendsen, H. J. C., Postma, J. P. M., van Gunsteren, W. F., DiNola, A., & Haak, J. R. (1984) *J. Chem. Phys. 81*, 3684–3690.

Bernstein, F. C., Koetzle, T. F., Williams, G. J. B., Meyer, E. F., Jr., Brice, M. D., Rodgers, J. M., Kennard, O., Shimanouchi, T., & Tasumi. M. (1977) *J. Mol. Biol. 122*, 535–542.

Bjorkman, P. J., & Parham, P. (1990) *Annu. Rev. Biochem. 59*, 253–288.

Boehncke, W.-H., Takeshita, T., Pendleton, C. D., Houghten, R. A., Scheherazade, S.-N., Racioppi, L., Berzofsky, J., & Germain, R. N. (1993) *J. Immunol. 150*, 331–341.

Burshtyn, D. N., & Barber, B. H. (1993) *J. Immunol. 151*, 3082–3093.

Callahan, T., Swanson, E., & Lybrand, T. (1993) QCPE Program No. 623, Indiana University, Bloomington, IN 47405.

Colbert, R. A., Rowland-Jones, S. L., McMichael, A. J., & Frelinger, J. A. (1993) *Proc. Natl. Acad. Sci. U.S.A. 90*, 6879–6883.

Connolly, M. L. (1983) *J. Appl. Crystallogr. 16*, 548–558 (QCPE Program No. 429).

Daser, A., Henning, U., & Henklein, P. (1994) *Mol. Immunol. 31*, 331–336.

Falk, K., Rötzschke, O., Stevanovic, S., Jung, G., & Rammensee, H. G. (1991) *Nature 351*, 290–296.

Fremont, D. H., Matsumura, M., Stura, E. C., Peterson, P. A., & Wilson, I. A. (1992) *Science 257*, 919–927.

Guo, H.-C., Jardetzky, T. S., Garrett, T. P. J., Lane, W. S., Strominger, J. L., & Wiley, D. C. (1992) *Nature 360*, 364–366.

Guo, H.-C., Madden, D. R., Silver, M. L., Jardetzky, T. S., Strominger, J. L., & Wiley, D. C. (1993) *Proc. Natl. Acad. Sci. U.S.A. 90*, 8053–8057.

Hill, A. V. S., Elvin, J., Willis, A. C., Aidoo, M., Allsopp, C. E. M., Gotch, F., Gao, M., Takiguchi, M., Greenwood, B. M., Townsend. A. R. M., McMichael, A. J. M., & Wittle, H. C. (1992) *Nature 360*, 434–439.

Huczko, E. L., Bodnar, W. M., Benjamin, D., Sakaguchi, K., Zhu, N. Z., Shabanowitz, J., Henderson, R. A., Appella, E., Hunt, D. F., & Engehard, V. H. (1993) *J. Immunol. 151*, 2572–2587.

Hunt, C., & Morimoto, R. O. (1985) *Proc. Natl. Acad. Sci. U.S.A. 82*, 6455–6459.

Hunt, D. F., Henderson, R. A., Shabanowitz, J., Sakaguchi, K., Michel, A., Sevilir, N., Cox, A. L., Appella, E., & Engelhard, V. H. (1992) *Science 255*, 1261–1263.

Jardetzky, T. S., Lane, W. S., Robinson, R. A., Madden, D. R., & Wiley, D. C. (1991) *Nature 353*, 326–329.

Jorgensen, W. L., Chandrasekhar, J., Madura, J. D., Impey, R. W., & Klein, M. (1983) *J. Chem. Phys. 70*, 926–935.

Karplus, M., & McCammon (1983) *Annu. Rev. Biochem. 53*, 263–300.

Karplus, M., & Petsko, G. A. (1990) *Nature 347*, 631–639.

Kingsley, G., & Sieper, J. (1993) *Immunol. Today 14*, 387–391.

Kitson, D. H., Avbelj, F., Moult, J., Nguyen, D. T., Mertz, J. E., Hadzi, D., & Hagler, A. T. (1993) *Proc. Natl. Acad. Sci. U.S.A. 90*, 8920–8924.

Krug, M. (1991) Ph.D. Thesis, University of Tübingen, Germany.

Madden, D. R., & Wiley, D. C. (1992) *Curr. Opin. Struct. Biol. 2*, 300–308.

Madden, D. R., Gorga, J. C., Strominger, J. L., & Wiley, D. C. (1992) *Cell 70*, 1035–1048.

Madden, D. R., Garboczi, D. N., & Wiley, D. C. (1993) *Cell 75*, 693–708.

Matsumura, M., Fremont, D. H., Peterson, P. A., & Wilson, I. A. (1992) *Science 257*, 928–934.

Pamer, E. G., Harty, J. T., & Bevan, M. J. (1991) *Nature 353*, 852–855.

Parker, K. C., Carreno, B., Sestak, B., Utz, U., Biddison, W. E., & Coligan, J. E. (1992a) *J. Biol. Chem. 267*, 5451–5459.

Parker, K. C., Dibrino, M., Hull, L., & Coligan, J. E. (1992b) *J. Immunol. 149*, 1896–1904.

Pearlman, D. A., Case, D. A., Caldwell, J. C., Seibel, G. L., Singh, C., Weiner, P., & Kollman, P. (1992) AMBER 4.0, University of California, San Francisco, CA.

Rammensee, H. G., Falk, K., & Rötzschke, O. (1993) *Annu. Rev. Immunol. 11*, 601–624.

Rognan, D., & Folkers, G. (1993) in *Trends in QSAR and Molecular Modeling 92* (Wermuth, C. G., Ed.) pp 186–192, ESCOM Science Publishers B.V., Leiden, The Netherlands.

Rognan, D., Reddehase, M. J., Koszinowski, U. H., & Folkers, G. (1992a) *Proteins: Struct., Funct., Genet. 13*, 70–85.

Rognan, D., Zimmermann, N., Jung, G., & Folkers, G. (1992b) *Eur. J. Biochem. 208*, 101–113.

Rötzschke, O., Falk, K., Stevanovic, S., Jung, G., Walden, P., & Rammensee, H. G. (1991) *Eur. J. Immunol. 21*, 2891–2894.

Rötzschke, O., Falk, K., Stevanovic, S., Gnau, V., Jung, G., & Rammensee, H. G. (1994) *Immunogenetics 39*, 74–77.

Ruppert, J., Sidney, J., Celis, E., Kubo, R. T., Grey, H. M., & Sette, A. (1993) *Cell 74*, 929–937.

Ryckaert, J. P., Cicotti, G., & Berendsen, H. J. C. (1977) *J. Comput. Phys. 23*, 327–341.

Saito, Y., Peterson, P. A., & Matsumura, M. (1993) *J. Biol. Chem. 268*, 21309–21317.
Saper, M. A., Bjorkman, P. J., & Wiley, D. C. (1991) *J. Mol. Biol. 219*, 277–319.
Silver, M. L., Guo, H.-C., Strominger, J. L., & Wiley, D. C. (1992) *Nature 360*, 367–369.
Townsend, A., & Bodmer, H. (1989) *Annu. Rev. Immunol. 7*, 601–624.
van Gunsteren, W. F., & Berendsen, H. J. C. (1990) *Angew. Chem., Int. Ed. Engl. 29*, 992–1023.
van Gunsteren, W. F., & Mark, A. E. (1992) *Eur. J. Biochem. 204*, 947–961.
Weiner, S. J., Kollmann, P. A., Case, D. A., Singh, U. C., Ghio, C., Alagona, G., Profeta, S., Jr., & Weiner, P. A. (1984) *J. Am. Chem. Soc. 106*, 765–784.
Young, A. C. M., Zhang, W., Sacchettini, J. C., & Nathenson, S. G. (1994) *Cell 76*, 39–50.
Zhang, W., Young, A. C. M., Imarai, M., Nathenson, S. G., & Sacchettini, J. C. (1992) *Proc. Natl. Acad. Sci. U.S.A. 89*, 8403–8407.
Zinkernagel, R., & Doherty, P. C. (1974) *Nature 90*, 701–702.
Zimmermann, N., Rötzschke, O., Falk, K., Rognan, D., Folkers, G., Rammensee, H. G., & Jung, G. (1992) *Angew. Chem., Int. Ed. Engl. 31*, 886–890.